Imaging the State-Specific Vibrational Predissociation of the Ammonia−Water Hydrogen-Bonded Dimer

Andrew K. Mollner, Blithe E. Casterline, Lee C. Ch'ng, and Hanna Reisler*

Department of Chemistry, University of Southern California, Los Angeles, California 90089-0482

Received: May 15, 2009; Revised Manuscript Received: August 7, 2009

The state-to-state vibrational predissociation (VP) dynamics of the hydrogen-bonded ammonia−water dimer were studied following excitation of the bound OH stretch. Velocity-map imaging (VMI) and resonance-enhanced multiphoton ionization (REMPI) were used to determine pair-correlated product energy distributions. Following vibrational excitation of the bound OH stretch fundamental, ammonia fragments were detected by $2 + 1$ REMPI via the $\tilde{B}^1E'' \leftarrow \tilde{X}^1A_1'$ transition. The REMPI spectra show that NH_3 is produced with one and two quanta of the symmetric bend (ν_2 umbrella mode) excitation, as well as in the ground vibrational state. Each band is quite congested, indicating population in a large number of rotational states. The fragments' center-of-mass (c.m.) translational energy distributions were determined from images of selected rotational levels of ammonia with zero, one, or two quanta in ν_2 and were converted to rotational state distributions of the water cofragment. All the distributions could be fit well by using a dimer dissociation energy of $D_0 = 1538 \pm 10$ cm^{-1}. The rotational state distributions in the water cofragment pair-correlated with specific rovibrational states of ammonia are broad and include all the J_{KaKc} states allowed by energy conservation. The rotational populations increase with decreasing c.m. translational energy. There is no evidence for ammonia products with significant excitation of the asymmetric bend (ν_4) or water products with bend (ν_2) excitation. The results show that only restricted pathways lead to predissociation, and these do not always give rise to the smallest possible translational energy release, as favored by momentum gap models.

1. Introduction

Understanding the nature, strength, and dynamics of hydrogen bonds has been a goal of physical chemistry research in the past century. Hydrogen bonding is critical to a wide range of chemical systems, from gas-phase dimers to condensed phase systems and complex biological molecules. In the gas phase, emphasis has been placed on studying hydrogen-bonded dimers in the cold environment of supersonic expansions. Experiments providing detailed state-specific information on the vibrational predissociation (VP) of hydrogen-bonded complexes primarily pertain to smaller hydrogen-bonded dimers containing at least one diatomic subunit such as a hydrogen halide.[1,2] In these systems, the disparity between the frequencies of the intramolecular and intermolecular vibrational modes causes energy transfer in the complex to be inefficient, leading to nonstatistical predissociation. For the predissociation of dimers containing two polyatomic molecules, state-specific information on energy disposal is scarce. The existence of low-frequency intramolecular vibrational modes in polyatomics may facilitate energy transfer in their complexes and lead to quite different predissociation behavior. Detailed studies of the predissociation of polyatomic hydrogen-bonded dimers are therefore critical for extending our understanding of hydrogen bonding to larger systems.

One such hydrogen-bonded dimer involving two polyatomic molecules that has been of considerable interest is that of ammonia and water (NH_3-H_2O). Mixtures of ammonia and water are important in a vast array of chemical fields, including industrial chemistry as a refrigerant,[3] in chemical evolution studies,[4] as a component of the surfaces of Neptune and Uranus,[5] in atmospheric chemistry,[6] and astrochemistry.[7−11] NH_3-H_2O represents also the simplest system containing the O−H···N hydrogen bonds ubiquitous in biological molecules. In fact, this was one of the earliest recognized hydrogen bonds, documented by Moore and Winmill in 1912 when studying the acidity of amines in aqueous solution.[12] As a result of its importance, NH_3-H_2O has been the subject of numerous theoretical[13−24] and experimental studies.[25−32]

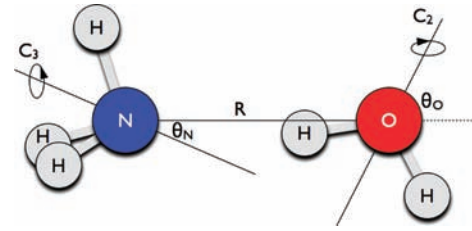

Figure 1. Equilibrium geometry of the ammonia−water dimer (ref. 32). $R(N-O) = 2.989$ Å; $\theta_N = 23.1°$; $\theta_O = 49.8°$.

The structure of NH_3-H_2O has been extensively studied both experimentally and theoretically. As shown in Figure 1, the equilibrium structure of the dimer has a slightly bent hydrogen bond ($\angle NHO \approx 170°$), with the water acting as hydrogen-bond donor to the nitrogen of ammonia and the free hydrogen of water in a trans position relative to the ammonia hydrogens. The most detailed structural study is the spectroscopic work of Stockman et al.[32] They found two structures that were consistent with the data, differing primarily in the angle between the C_{3v} axis and a-axis of the dimer (θ_N). On the basis of the available ab initio calculations at the time, the authors preferred the structure with the smaller value of θ_N (Stockman et al. structure a). More sophisticated calculations performed later have shown that the larger value of $\theta_N = 23.1°$ (Stockman et al. structure b) is likely the true equilibrium structure.[18] Although Figure 1 represents

* To whom correspondence should be addressed. E-mail: reisler@usc.edu. Phone: 213-740-7071. Fax: 213-740-3972.

10.1021/jp904566w CCC: $40.75
Published on Web 08/28/2009

the lowest-energy equilibrium structure, NH_3-H_2O is far from rigid. The NH_3 monomer is nearly free to rotate, with the rotation barrier through the cis configuration estimated to be 10.5 cm^{-1} spectroscopically[32] and calculations giving 0.1−2.2 cm^{-1}.[19,20] Exchange of the water hydrogens is also possible, but the barrier (700−1300 cm^{-1}) and minimum-energy pathway are less well-established.[19,32]

The infrared (IR) spectrum of NH_3-H_2O was first measured in low-temperature matrixes.[25−27] The most prominent feature of these spectra was the large red-shift of about 300 cm^{-1} for the bound OH stretch frequency relative to that of the monomer. The observed frequency of the bound OH stretch ranged from 3412 to 3456 cm^{-1} depending upon the nature of the matrix. More recently, the infrared spectrum of NH_3-H_2O was investigated in He droplets,[28] where perturbations by He are minimal. The observed bound OH stretch frequency of 3480 cm^{-1} should therefore be close to the expected gas-phase value. Ab initio calculations confirm that the dominant change in monomer frequencies upon complexation is the red-shift of the bound OH stretch (shift ≈ -200 cm^{-1}), with smaller blue-shifts of the ammonia bend (shift ≈ 50 cm^{-1}) and water bend (shift ≈ 40 cm^{-1}), whereas all other intramolecular modes are only slightly perturbed.[18,20] In addition, four intermolecular modes below 200 cm^{-1} have been calculated: the intermolecular stretch (199 cm^{-1}), NH_3 wag (166 and 175 cm^{-1}), and NH_3 torsion (19 cm^{-1}).[20]

Despite the large amount of interest in NH_3-H_2O, there has been no experimental determination of the strength of its hydrogen bond. The large red-shift of the bound OH stretch indicates that the hydrogen bond is relatively strong. Fraser and Suenram[29] observed that the dimer does not dissociate upon excitation of the NH_3 symmetric bend (ν_2 umbrella mode), indicating that the dissociation energy is greater than 1021 cm^{-1}. There have been a number of ab initio calculations of the binding energy, with quite good agreement among recent calculations.[18−20] Sadlej et al. calculated the energy (using MP2/AVQZ theory/basis) at the optimized geometry (MP2/AVTZ) with zero-point vibrational energy corrections (MP2/AVTZ). Their best estimate of D_0 was 4.149 kcal mol^{-1} (1451 cm^{-1}). Lane et al. reported a binding energy calculated with the CCSD(T)/AVQZ theory/basis including zero-point vibrational energy correction (CCSD(T)/AVTZ) to yield a best estimate of $D_0 = 4.20$ kcal mol^{-1} (1470 cm^{-1}).

In our previous studies of VP at the pair-correlated level for the hydrogen-bonded dimers H(D)Cl−acetylene and NH_3−acetylene we have exploited the imaging technique.[33−35] Both dimers provided clear evidence for state-specific VP dynamics. In particular, for the NH_3−acetylene dimer products were only observed with vibrational excitation in specific modes. All ammonia products observed had some excitation of ν_2 with the main predissociation channel being $NH_3(1\nu_2) + C_2H_2(2\nu_4$ or $1\nu_4 + 1\nu_5)$ where ν_4 and ν_5 are bending modes. There are two main differences between the hydrogen bonds in NH_3−acetylene and NH_3-H_2O: (i) whereas the NH_3−acetylene hydrogen bond is linear, the NH_3-H_2O hydrogen bond is slightly bent, and (ii) the hydrogen bond in NH_3-H_2O is expected to be significantly stronger than that in NH_3−acetylene (900 ± 10 cm^{-1})[34] due to the stronger acidity of water. A primary motivation for the experiments described here was to determine how these differences affect energy flow patterns and the VP mechanism.

In this paper, we report the first VP study of NH_3-H_2O. Complexes were formed in a pulsed molecular beam and the bound OH stretch was excited by a pulsed IR laser to induce vibrational predissociation. Resonance-enhanced multiphoton ionization (REMPI) was used to detect the ammonia fragments. We used the ammonia REMPI spectrum to determine ammonia state distributions and velocity-map imaging (VMI) to obtain energy distributions of water fragments pair-correlated with specific rovibrational states of ammonia. The observed state distributions were less state-specific than those observed previously in NH_3−acetylene, with population observed in all energetically accessible NH_3 ν_2 levels, as well as its ground vibrational state. However, other levels that are energetically allowed and give rise to low translational energy release, namely, the asymmetric ammonia bend and the water bend, have only a little, if any, population. A detailed analysis of pair-correlated state distributions was complicated by the highly congested ammonia REMPI spectrum and the large number of water rotational states available. Nevertheless, several general trends emerged, and the dimer's dissociation energy was determined to be $D_0 = 1538 \pm 10$ cm^{-1}.

2. Experimental Details

Vibrational predissociation of NH_3-H_2O formed in a pulsed supersonic molecular beam was studied following pulsed IR laser excitation. Rotationally excited NH_3 fragments were ionized by 2 + 1 REMPI and detected by time-of-flight (TOF) mass spectroscopy and VMI. The experimental procedures were similar to those used in our studies of HCl−acetylene and NH_3−acetylene.[33,34]

The dimers were formed in a pulsed supersonic molecular beam by expanding a mixture of 0.75% water and 1.5% ammonia (Matheson, anhydrous 99.99%) in He (Gilmore, 99.9999%) at a stagnation pressure of ∼1.5 atm through the 0.5 mm orifice of a pulsed valve (150 μs opening time) operating at 10 Hz. Samples were prepared by transferring water by vacuum distillation to an evacuated bulb followed by adding gaseous ammonia. The concentrations were optimized to minimize contamination from larger clusters of ammonia and ammonia−water. Dimer formation was not found to be critically dependent on gas concentrations or backing pressure; however, contributions from larger clusters increased dramatically at higher gas concentrations (see below). The skimmed molecular beam was intersected at right angles by two counterpropagating laser beams in the interaction region.

Unfocused IR laser radiation (∼5 mJ/pulse) was used to excite the bound OH stretch of the dimer (3485 cm^{-1}), and focused (focal length = 40 cm) frequency-doubled (Inrad Autotracker III) ultraviolet (UV) radiation (0.5 mJ; ∼0.4 cm^{-1} linewidth) was used to ionize state-selected ammonia fragments from the vibrational predissociation of the dimer. The IR radiation was generated by an OPO/OPA system (LaserVision, up to 22 mJ; 0.4 cm^{-1} linewidth). The IR frequency was calibrated using the absorption spectra of gaseous CH_4 and H_2O. The UV radiation was generated by a dye laser (Continuum ND 6000, LDS 698) pumped by a Nd:YAG laser (Continuum Surelite-III) and frequency calibrated by the known REMPI spectrum of NH_3 (see below). The timing of the lasers was adjusted by a delay generator (Stanford, DG535) controlled through a GPIB interface (National Instruments). Spectra were collected by alternating "IR on" and "IR off" conditions at each frequency. In "IR on", the IR laser fired 50 ns before the UV laser, whereas in "IR off", the IR laser was fired 1 μs after the UV laser. Laser conditions were optimized to minimize multiphoton signal contributions from larger clusters.

The timing of the lasers' firings was carefully optimized to excite dimers in the later part of the molecular beam pulse,

where their highest relative abundance was found. The rotational temperature of the background ammonia was estimated to be 5−10 K by monitoring the origin band of the $\tilde{B}^1E'' \leftarrow \tilde{X}^1A_1'$ system of monomer ammonia by 2 + 1 REMPI.[36] The UV spectra were modeled using the program PGOPHER[37] developed by Western with rotational constants from Cottaz et al.[38] For $\nu_2 = 0^+$, $B = 9.95$ cm^{-1}, and $C = 6.23$ cm^{-1}. The well-known origin band positions were used to calibrate the UV wavelength. Vibrationally excited ammonia fragments were detected through the same $\tilde{B}$ state in the range of 342.1−347.8 nm. A small background signal from vibrationally excited ammonia was also observed, indicating that vibrational cooling was not as efficient as rotational cooling.

The VMI arrangement has been described in detail previously.[39,40] In brief, it consists of a four-lens ion acceleration assembly, a 60 cm field-free drift tube, and a CCD camera (LaVision, Imager) that monitors a phosphor screen coupled to a microchannel plate (MCP) detector (BURLE Electro-Optics Co.). In this experiment, two modes were used to collect data: (i) TOF mass spectrometry for spectroscopic investigations and (ii) VMI mode for determining center-of-mass (c.m.) translational energy distributions. The two-dimensional projections were collected using an event counting method (DaVis) and reconstructed to three-dimensional images by using the BASEX method,[41] which also provided the speed distributions after summing over the angular distribution for each radius. Speed (radial distance) distributions were converted to c.m. translational energy distributions by using momentum conservation and calibration constants obtained by imaging photodissociation products from the well-known I_2, NO_2, and O_2 systems.[42−44] The translational energy distributions were analyzed to determine the internal energy of the water cofragments as well as the dissociation threshold of NH_3-H_2O.

3. Results and Analysis

3.1. Infrared Action Spectra. We obtained IR spectra of the dimer in the range of the bound OH stretch fundamental by monitoring NH_3 photofragments in selected rovibrational states by REMPI while scanning the IR laser frequency. IR spectra measured at 3340−3510 cm^{-1} under varying conditions are shown in Figure 2. The data shown are the enhancement of the NH_3^+ signal following IR excitation and have the background NH_3^+ signal with the IR laser off subtracted. It is important to note that these are "action" spectra; in order to observe signal not only must there be absorption of IR photons, but this absorption must lead to the production of NH_3 fragments in the specific rovibrational state being monitored. The traces shown in Figure 2 were obtained by monitoring $NH_3(\nu_2 = 1^+, J = 1$ or 3). Similar spectra were observed monitoring $NH_3(\nu_2 = 2^+)$. Spectra taken monitoring $NH_3(\nu_2 = 0^+)$ were qualitatively similar but much noisier due to the larger background signal.

In the process of optimizing the dimer signal, IR scans were taken with many combinations of gas concentrations and laser powers. Figure 2 shows three survey IR scans which represent an illustrative range of conditions. The top trace, taken under conditions of high IR laser fluence (5 mJ; focal length = 40 cm) and high water and ammonia concentrations (1% water, 3% ammonia), shows significant enhancements throughout this region, dominated by a peak around 3410 cm^{-1}. When the concentrations were decreased (e.g., 0.6% water, 1.25% ammonia; middle trace), the intensity of the 3410 cm^{-1} peak also decreased, leaving a broad absorption throughout the scanned region with smaller peaks at 3445 and 3485 cm^{-1}. When the IR laser fluence was also decreased (3 mJ unfocused; bottom trace), NH_3 fragments from multiphoton dissociation of larger clusters containing ammonia were minimized, and the feature centered at ∼3485 cm^{-1} became the prominent spectral feature. As discussed below, we assign this absorption to the bound OH stretch of NH_3-H_2O. The smaller two peaks at ∼3430 cm^{-1} correspond to the ammonia dimer.[31]

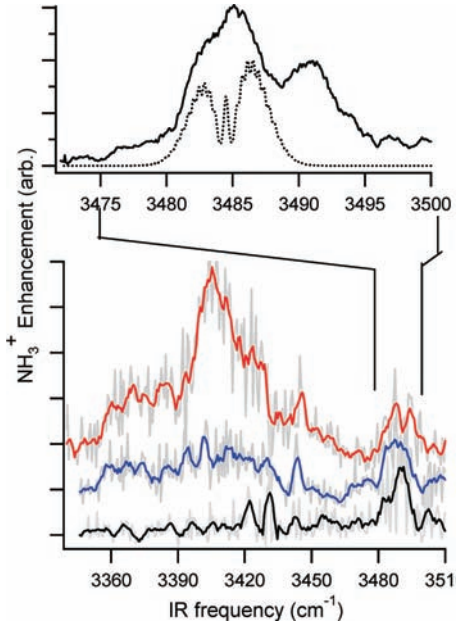

Figure 2. $NH_3(\nu_2 = 1^+; J = 1-3)$ fragment yield IR spectra of NH_3-containing clusters. Survey scans were taken at high concentration and IR power (top, red), low concentration and high IR power (middle, blue), and low power and concentration (bottom, black). See the text for details. Colored lines have been smoothed to the resolution of our laser (0.4 cm^{-1}). The inset shows the average of 15 scans of the peak assigned to NH_3-H_2O taken with 3−5 mJ IR power (unfocused), 0.75% water, 1.5% ammonia, and 1.5 atm stagnation pressure. The dotted curve is the simulation of an *a*-type band with rotational temperature of 10 K, fwhm = 0.4 cm^{-1}, and published rotational constants (ref. 32).

The inset in Figure 2 shows the average of several scans of the NH_3-H_2O peak recorded under optimized conditions (0.75% water, 1.5% ammonia, 1.5 atm of stagnation pressure, 3−5 mJ of unfocused IR). This peak is well-separated from the signals from larger clusters at lower frequencies. The observed peak profile has a 12 cm^{-1} width and no resolvable rotational structure. It consists of two subpeaks whose relative intensity, but not positions or shapes, vary with experimental conditions. The most significant variation was with IR laser fluence, with the high-frequency peak growing faster than the low-frequency peak as IR fluence increased. Changing the beam conditions to vary the temperature of the expansion produced no observable change in the relative intensity of the two peaks. A careful inspection of the product NH_3 REMPI spectrum upon changing the IR frequency from the low-frequency peak to the high-frequency peak indicated no significant change in relative NH_3 product state distributions. As discussed below, we believe that the high-frequency peak is due to combination bands present in internally excited dimers. To avoid potential overlap, all data reported below were obtained with the IR frequencies fixed on the low-frequency peak centered at 3485 cm^{-1}.

3.2. REMPI Spectroscopy of Ammonia Fragments. Figure 3 shows all the monomer vibrational modes that are available for energy disposal given our excitation energy and measured D_0. REMPI spectra of NH_3 fragments produced from the VP of NH_3-H_2O at 3485 cm^{-1} are shown in Figures 4 and 5. The spectra clearly show bands corresponding to NH_3 produced with

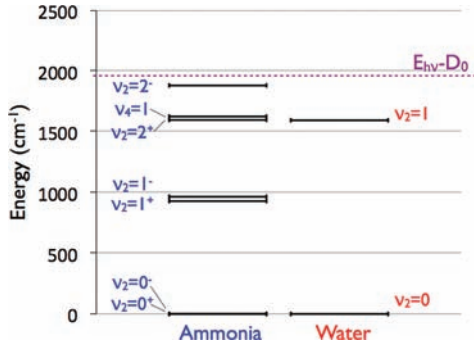

Figure 3. Accessible vibrational levels in the monomer fragments following vibrational predissociation. $E_{h\nu} - D_0 = 3485 - 1538 = 1947$ cm^{-1}.

umbrella bending mode (ν_2) excitation, as well as in the ground vibrational state. Each band is quite congested, indicating population in a large number of rotational states.

Due to the large amount of energy deposited into NH_3 $\nu_2 = 2^+$ (1597.5 cm^{-1}), the $\tilde{B}(\nu_2 = 0) \leftarrow \tilde{X}(\nu_2 = 2^+)$ band (Figure 5a) has the fewest number of allowed rotational states and is the least congested. The spectrum was simulated with a rotational temperature of 300 K and $J \leq 7$. The peak positions and relative heights are simulated quite well, indicating the NH_3 rotational state distribution for this band is Boltzmann-like, truncated at the highest rotational level allowed by energy conservation. However, the spectrum is too congested to extract a more detailed rotational state distribution. In this region, no evidence was found for the $\tilde{B}(\nu_4 = 0) \leftarrow \tilde{X}(\nu_4 = 1)$ transition, even though population of the ammonia asymmetric bend is energetically allowed (see Figure 3). Although the $\tilde{B}(\nu_4 = 0) \leftarrow \tilde{X}(\nu_4 = 1)$ REMPI spectrum is expected to have a sharp Q-branch peak around 57 600 cm^{-1}, the relative strength of this transition could be much lower than for $\tilde{B}(\nu_2 = 0) \leftarrow \tilde{X}(\nu_2 = 2^+)$, so some production of NH_3 with one quantum in ν_4 cannot be ruled out.

The REMPI spectrum of NH_3 product fragments in the region of the $\tilde{B}(\nu_2 = 0) \leftarrow \tilde{X}(\nu_2 = 1^+)$ band is shown in Figure 5b. The best simulation for this spectrum was with a rotational temperature of 400 K and $J \leq 13$. No clear evidence was seen for the energy- and symmetry-allowed $\tilde{B}(\nu_2 = 1) \leftarrow \tilde{X}(\nu_2 = 2^-)$ transition in this region (Figure 3). However, considering the value of D_0, we expect only very few rotational states and those peaks would be buried beneath the dense forest of peaks observed for the $\tilde{B}(\nu_2 = 0) \leftarrow \tilde{X}(\nu_2 = 1^+)$ transition.

The region corresponding to the $\tilde{B}(\nu_2 = 0) \leftarrow \tilde{X}(\nu_2 = 0^+)$ transition is shown in Figure 5c. The signal-to-noise of the enhancement spectrum in this region was degraded due to the much larger monomer signal obtained with the IR laser off. In addition, enhancement from 59 210 to 59 360 cm^{-1} could not be measured due to very strong transitions from low-J levels of monomer NH_3. Analysis in this region was further complicated by the large amount of energy available for NH_3 rotation as well as the overlap of two other allowed transitions, $\tilde{B}(\nu_2 = 1) \leftarrow \tilde{X}(\nu_2 = 1^-)$ and $\tilde{B}(\nu_2 = 2) \leftarrow \tilde{X}(\nu_2 = 2^+)$. Shown in Figure 5c is a simulation with a rotational temperature of 300 K. No combination of temperatures and intensities for the three allowed transitions was found to adequately reproduce the observed spectrum, and the rotational state distributions for NH_3 formed in $\nu_2 = 0^+$ appear to be poorly described by a Boltzmann distribution. This may be partly a result of the blended nature of the transitions.

The NH_3 bands of (−) symmetry are not resolved, although the high density of rotational states near 59 100 cm^{-1} is likely due to contributions from $\tilde{B}(\nu_2 = 1) \leftarrow \tilde{X}(\nu_2 = 1^-)$. No state specificity regarding the two symmetry components of the umbrella mode is expected, in analogy with observations of the NH_3−acetylene dimer.[34] However, it is difficult to see these (−) bands via the $\tilde{C} \leftarrow \tilde{X}$ transition used previously because of much greater congestion and overlap.

3.3. Ion Imaging Results and Analysis. VMI data monitoring state-selected NH_3 photofragments are shown in Figures 6−9. Photofragment images were obtained for state-selected NH_3 in $\nu_2 = 0^+$, 1^+, and 2^+. The angular distributions in all images were isotropic, as illustrated by the unreconstructed image in Figure 6 taken by monitoring $\nu_2 = 2^+$, $J = 3$. Figure 6 also shows the BASEX reconstruction, plotted in velocity (pixel) space, of this image. The size of the image in pixels is proportional to the radial distance from the center and to the speed. Images of NH_3 fragments with less vibrational excitation are larger, with $\nu_2 = 0^+$ fragment image radii on the order of 150 pixels. The speed distributions were then converted to c.m. translational energy distributions, and typical examples are shown in Figures 7−9.

To determine the correlated internal state distributions of the water fragment, conservation of energy was used:

$$E_{int}(NH_3{-}H_2O) + h\nu = D_0 + E_T + E_{vib}(NH_3) + E_{vib}(H_2O) + E_{rot}(NH_3) + E_{rot}(H_2O)$$

where $E_{int}(NH_3{-}H_2O)$ is the internal energy of the dimer prior to excitation, $h\nu$ is the photon energy used for vibrational excitation of the dimer (3485 cm^{-1}), D_0 is the dissociation energy of the dimer, E_T is the c.m. translational energy, $E_{vib}(NH_3)$ and $E_{vib}(H_2O)$ are the vibrational energies of ammonia and water, respectively, and $E_{rot}(NH_3)$ and $E_{rot}(H_2O)$ are the corresponding rotational energies. $E_{int}(NH_3{-}H_2O)$ is estimated to be 5 cm^{-1} (see below). State-selective REMPI defines $E_{rot}(NH_3)$ and $E_{vib}(NH_3)$, and E_T is determined from the images. This leaves D_0, $E_{vib}(H_2O)$, and $E_{rot}(H_2O)$ as unknowns, although for images with NH_3 bending excitation $E_{vib}(H_2O)$ must be zero due to conservation of energy.

Reconstructed images in velocity (pixels) space were used to determine the rotational level populations of pair-correlated water fragments. This procedure improves our ability to resolve structures at low E_T and identify the maximum observed E_T (compare Figures 6 and 7). Fitting was accomplished by assigning a Gaussian-shaped curve to each rovibrational state of H_2O,[45] with a width characteristic of our experimental resolution. The positions of these Gaussians were then shifted together by adjusting D_0 until both the observed structure and maximum E_T were best matched. The heights of the Gaussians were described by a smooth function of E_T and then adjusted to fit structural features at low E_T.

Every effort was made to monitor single rovibrational states of NH_3. Given the complexity of the REMPI spectra, this was a major challenge. We were most successful with $NH_3(\nu_2 = 2^+)$. Characterizing the selected transitions with ${}^{\Delta K}\Delta J_K(J)$ notation, images were recorded by monitoring the ${}^rS_0(3)$, ${}^rR_3(3)$, and ${}^rR_6(6)$ at 57 790, 57 634, and 57 618 cm^{-1}, respectively. Despite their differing amounts of NH_3 rotational energy, all three images were best fit with a consistent D_0 of 1537 ± 2 cm^{-1}. The ${}^rS_0(3)$ image along with its fit is shown in Figure 6, and the corresponding c.m. translational energy distributions, $P(E_T)$, along with the normalized state distribution for the pair-correlated H_2O rotational states are shown in Figure 7.

For NH_3 with $\nu_2 = 1^+$ we were also able to fit images from three isolated states: ${}^rS_0(3)$, ${}^rS_0(5)$, and ${}^rS_1(2)$ at 58 459, 58 537,

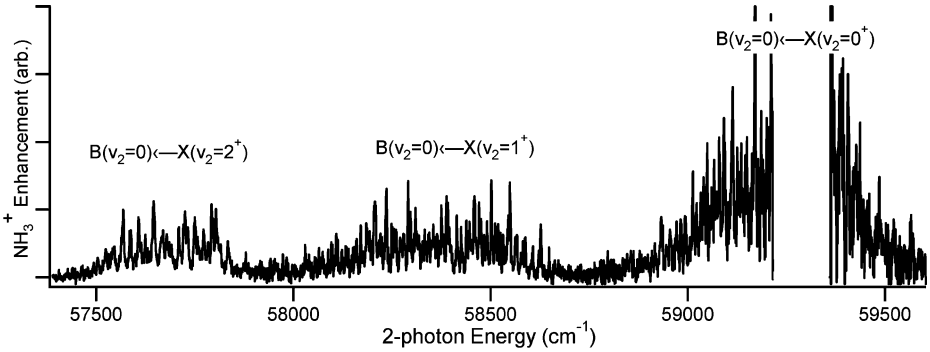

Figure 4. NH_3 photofragment 2 + 1 REMPI survey spectrum obtained by exciting the bound OH stretch of NH_3-H_2O at 3485 cm^{-1} and scanning the UV laser through several $\tilde{B}^1E'' \leftarrow \tilde{X}^1A_1'$ transitions of NH_3. Data shown have had the "IR off" background subtracted. The gap in the data corresponds to the region of low-J transitions from $\nu_2 = 0^+$ for which the background intensity was too large to measure enhancement. Each band is labeled with the predominant vibronic transition. See the text for details.

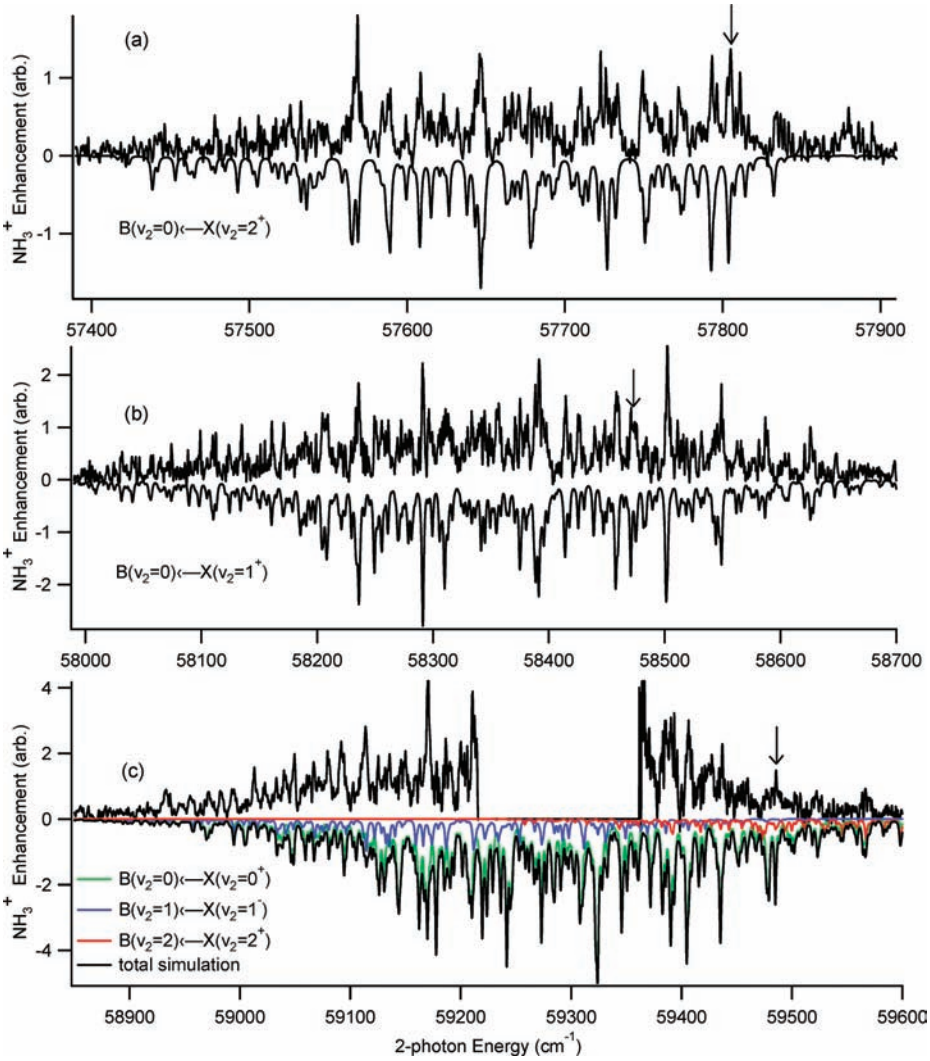

Figure 5. NH_3 photofragment 2 + 1 REMPI spectra following excitation of the bound OH stretch of NH_3-H_2O at 3485 cm^{-1} (upper curves) and PGOPHER simulations (lower curves). (a) $NH_3(\nu_2 = 2^+)$; (b) $NH_3(\nu_2 = 1^+)$; (c) overlapping transitions from $NH_3(\nu_2 = 0^+, 1^-,$ and $2^+)$. The gap in the data corresponds to the region of low-J transitions from $\nu_2 = 0^+$ for which the background intensity was too large to measure enhancement. The arrows mark peaks monitored for the images shown in Figures 6−9.

and 58 406 cm^{-1}, respectively. Although the structure in these images was not as prominent as those for $\nu_2 = 2^+$, again all three images could be fit unambiguously with a consistent D_0 of 1541 ± 5 cm^{-1}. The c.m. $P(E_T)$ obtained by monitoring the $^rS_0(3)$ transition along with its fit and the normalized state distribution for the pair-correlated H_2O rotational states are shown in Figure 8.

For NH_3 with $\nu_2 = 0^+$ the challenge of finding a REMPI transition for an isolated rovibrational line was much greater. We took images of several peaks in the low-frequency tail of the band. These images had tails extending to the high E_T expected for NH_3 in the vibrational ground state, but no discernible structure, most likely due to overlap of multiple transitions with $\nu_2 = 0^+$, $\nu_2 = 1^-$, or $\nu_2 = 2^+$. At higher

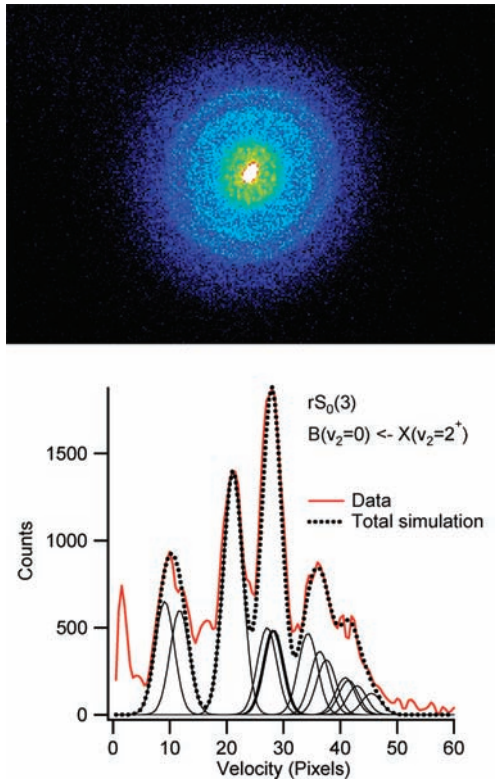

Figure 6. Unreconstructed image (top) and the corresponding velocity distribution derived from the BASEX-reconstructed image (bottom) of state-selected $NH_3(\nu_2 = 2^+, J = 3, K = 0)$ fragments produced in the vibrational predissociation of NH_3-H_2O plotted in units of pixels (proportional to velocity). Positions of Gaussians used in the simulation were determined by known H_2O rotational energies and the fit parameter D_0. The widths of the Gaussians are determined by the experimental resolution.

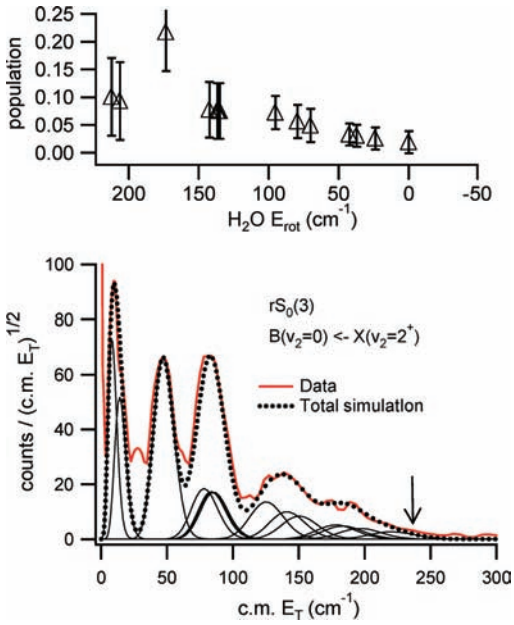

Figure 7. Fragment translational energy distribution (c.m.) obtained by monitoring $NH_3(\nu_2 = 2^+, J = 3, K = 0)$ via the $^rS_0(3)$ line of the $\tilde{B} \leftarrow \tilde{X}$ transition and simulation (see text for details). The arrow indicates the maximum available translational energy for $D_0 = 1538$ cm^{-1}. The top panel shows the normalized relative populations of the water rotational states used to fit the data. The *x*-axis has been inverted such that the states line up vertically with the corresponding features in the c.m. translational energy distribution.

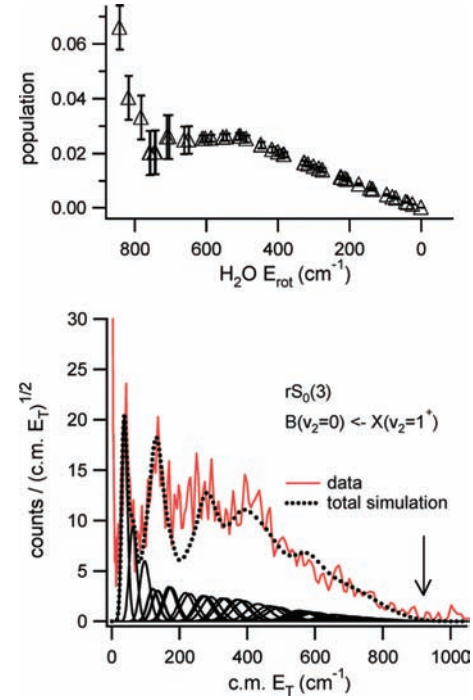

Figure 8. Fragment translational energy distribution (c.m.) obtained by monitoring $NH_3(\nu_2 = 1^+, J = 3, K = 0)$ via the $^rS_0(3)$ line of the $\tilde{B} \leftarrow \tilde{X}$ transition and simulation (see text for details). The arrow indicates the maximum available translational energy for $D_0 = 1538$ cm^{-1}. The top panel shows the normalized relative populations of the water rotational states used to fit the data. The *x*-axis has been inverted such that the states line up vertically with the corresponding features in the c.m. translational energy distribution.

frequencies, transitions from $\nu_2 = 1^-$ no longer contribute, and we were able to record an image that is dominated by the $^rS_0(5)$ transition from $\nu_2 = 0^+$. This image shows clear structure at low E_T but much less structure at higher E_T than expected from the simulations. This is likely due to some persisting overlap of other transitions. Using the structure at low E_T and the maximum E_T observed, the image was fit with $D_0 = 1539 \pm 5$ cm^{-1}. The corresponding c.m. $P(E_T)$ along with its fit and the normalized state distribution of the correlated H_2O rotational states are shown in Figure 9. For this state, the available energy is $h\nu - D_0 - E_{rot}(NH_3) = 3485 - 1539 - 298 = 1648$ cm^{-1}, sufficient to populate the bending mode of water ($E(010) = 1595$ cm^{-1}). Unfortunately, the internal energy of the allowed water rotational states associated with $NH_3(J = 5)$ and one quantum of water bend (1595, 1619, 1635 cm^{-1}) are nearly degenerate with water rotational states with no bending excitation (1591, 1616, 1631 cm^{-1}), so a direct analysis of the bending mode population could not be made. The filled triangles in Figure 9 represent those states that could include contributions from water bend.

4. Discussion

4.1. Infrared Spectrum of Ammonia−Water Clusters. To date, no high-resolution gas-phase spectra of the bound OH stretch region of NH_3-H_2O have been published. Thus, a definite correlation between the observed NH_3 photofragment action spectra and dimer absorption features needs to be established. Our survey scans (Figure 2) obtained by monitoring NH_3 in $\nu_2 = 1^+$ and 2^+ show large enhancements upon IR excitation at 3360−3480 cm^{-1} that depend on the monomer concentrations and laser power. Because we measure the

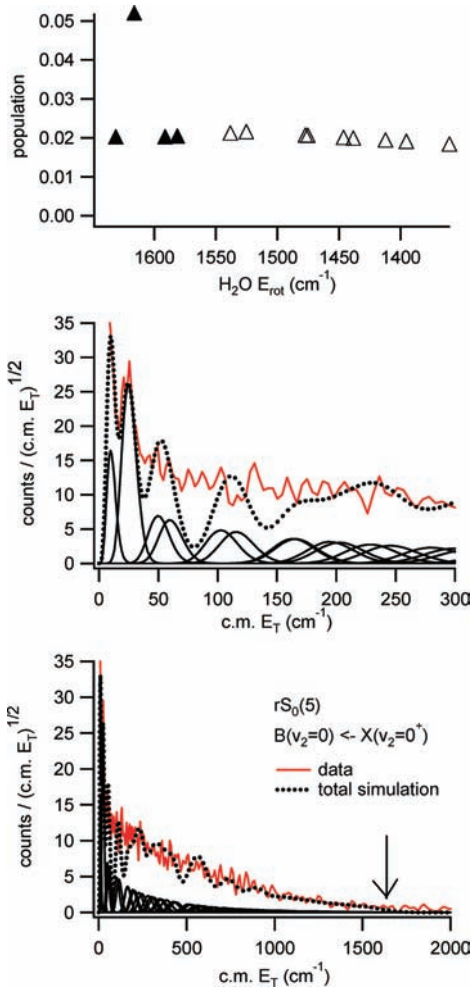

Figure 9. Fragment translational energy distribution (c.m.) obtained by monitoring $NH_3(\nu_2 = 0^+, J = 5, K = 0)$ via the $^rS_0(5)$ line of the $\tilde{B} \leftarrow \tilde{X}$ transition and simulation (see text for details). The arrow indicates the maximum available translational energy for $D_0 = 1538$ cm^{-1}. The middle panel shows the lowest E_T region of the data, and the top panel shows the normalized relative populations of the corresponding water rotational states used to fit the data. The *x*-axis has been inverted such that the states line up vertically with the corresponding features in the c.m. translational energy distribution.

enhancement of NH_3 REMPI signal following IR excitation, this signal must be due to IR absorption by NH_3-containing complexes.

The strong concentration dependence of the prominent feature at 3410 cm^{-1} indicates this is absorption by larger $(NH_3)_x(H_2O)_y$ complexes. Complexes of pure $(NH_3)_x$ have previously been observed in He droplets at 3420 cm^{-1} ($x = 2$) and 3400 cm^{-1} ($x = 3$),[31] and these likely contribute. In addition, a fairly broad absorption due to pure water tetramers was observed at 3400 cm^{-1};[34] thus, some signal could arise from the dissociation of $(NH_3)_x(H_2O)_4$, which may absorb in the same region. The signal that remains at lower concentrations, but requires higher IR laser fluence, likely arises from multiphoton dissociation of small mixed complexes. Calculations for the mixed trimers $(NH_3)_2(H_2O)_1$ and $(NH_3)_1(H_2O)_2$ indicate that the hydrogen bonding is stronger than for the dimer, exceeding the IR photon energy.[19] This would prevent photodissociation by a single photon and would likely lead to a larger red-shift of the bound OH stretch from that of the dimer. For example, in matrices Yeo and Ford[27] assigned a peak red-shifted by ~40 cm^{-1} with respect to the dimer's OH stretch peak to $(NH_3)_1(H_2O)_2$. In our spectra, this would correspond to the peak at ~3440 cm^{-1}, which is prominent in all spectra recorded with high laser intensity. In conclusion, we assign the absorption feature at 3485 cm^{-1} to the bound OH stretch of NH_3-H_2O, on the basis of its behavior with respect to changes in laser power and concentration and its similarity to the NH_3-H_2O dimer peak in He droplets.[28]

We turn now to the shoulder observed in the high-frequency wing of the dimer peak at 3485 cm^{-1}. Included as an inset in Figure 2 is a simulation of the dimer band profile using published rotational constants from Stockman et al.[32] and assuming an *a*-type transition, Gaussian fwhm of 0.4 cm^{-1}, and rotational temperature of 10 K (obtained by Asyrot[46]). Although the simulation indicates that, at our laser resolution, no rotational fine structure should be seen, a clear P-, Q-, R-branch structure should be resolvable with an overall width consistent with only one of the observed peaks (<10 cm^{-1}). In addition, the spectra observed in He droplets showed only a single peak at this location, even when larger clusters were present. This suggests that both peaks can be attributed to NH_3-H_2O and that one is likely due to higher internal energies in our experiment relative to the He droplet experiments. Although we expect dimers formed in our expansion to be rotationally cold, the vibrational cooling may be less efficient. Ab initio calculations yield several modes of the dimer below 200 cm^{-1} including motions of the NH_3 subunit and the intermolecular stretch. Population of some of these modes may slightly weaken the hydrogen bond and lead to a less red-shifted bound OH stretch.[47] The overlap of transitions with slightly different red-shifts may also explain why we observe no rotational branches. However, we cannot offer a conclusive assignment for the high-frequency peak.

A careful examination of the simulated rotational band at 10 K indicates that it is dominated by transitions with $J \leq 10$ and $K_a = 0$ or 1. This is consistent with the previous spectroscopic study conducted in a molecular beam by Fraser and Suenram[29] who observed dominant transitions from $K_a = 0$ or 1 when exciting to the NH_3 umbrella mode in the dimer. Because we see no substructure, it is difficult to assign a specific rotational state or energy to the dimers in our beam. Our IR frequency was generally set to be near or just to the red of the peak centered at 3485 cm^{-1}. We therefore were likely exciting dimers in the range $0 \leq J \leq 5$ and $K_a = 0$ or 1. This gives a total range of dimer internal energies of 0−10 cm^{-1}. If we assume a Boltzmann-like distribution of rotational states at 10 K then the weighted average internal energy of our excited dimers is about 5 cm^{-1}. In our final analysis of D_0 we therefore use $E_{int}(NH_3-H_2O) = 5 \pm 5$ cm^{-1}.

With no observed rotational fine structure, we cannot make a direct estimate of the lifetime of excited NH_3-H_2O. Similar hydrogen-bonded complexes have been shown to live for many vibrational periods in the excited state before dissociation. The lifetime of NH_3−acetylene following excitation of the asymmetric CH stretch was estimated to be >0.1 ns.[48] The lifetimes of $(H_2O)_2$ and $(D_2O)_2$ following excitation of the bound OH stretch were found to be 80 ps and 5 ns, respectively.[49] Similarly, we expect the lifetime of excited NH_3-H_2O to be longer than 10 ps.

4.2. Dissociation Energy of the Ammonia−Water Dimer. Several factors give us confidence in the accuracy of our measured D_0 for NH_3-H_2O. The most important of these is the consistency of D_0 used to fit images taken by monitoring a range of different rovibrational states of ammonia. All images for which we could resolve some rotational structure of the water cofragment were fit with D_0 within a range of 10 cm^{-1}.

Additional images taken by monitoring overlapped $NH_3(\nu, J)$ states for which no rotational structure was resolved still had maximum E_T consistent with our measured D_0. The NH_3 REMPI spectra also support our D_0, as the maximum J observed in each vibronic band is consistent with a D_0 around 1540 cm^{-1}.

The D_0 derived from an individual image fit is quite narrowly constrained by the structure. The finite width of observed peaks places a lower limit on our fitting uncertainty at ± 1 cm^{-1} and the uncertainty can be as high as 6 cm^{-1}, depending on the signal-to-noise. The D_0 values and uncertainties quoted above for each vibrational band of ammonia are weighted averages for all images fit in that band. The calibration constant used to convert images from pixels to translational energy has an uncertainty of ~5%. However, an error in these calibration constants would impact our ability to simultaneously fit peaks at different E_T and is probably reflected in our fit uncertainties. The largest systematic uncertainties stem from the internal energy of the dimer prior to excitation and the calibration of our IR laser frequency. As discussed above, the uncertainty in $E_{int}(NH_3-H_2O)$ is estimated to be 5 cm^{-1}. From our calibrations, we estimate the uncertainty in the IR frequency in this region to be on the order of 1 cm^{-1}. Taking a weighted average of all our data and combining random and systematic uncertainties, we arrive at a value of $D_0 = 1538 \pm 10$ cm^{-1}.

To our knowledge, the only previous experimental information about D_0 was from the microwave−infrared double-resonance experiment of Fraser and Suenram,[29] who observed no dissociation of the dimer and therefore placed a lower limit on the dissociation energy of 1021 cm^{-1}. They suggested that excitation of ν_2 in ammonia might lower the dissociation energy of the dimer. Although we cannot rule out some small effect, our data do not show any systematic variation in D_0 with product ν_2 population outside our measurement uncertainties.

Our measured D_0 can also be used as a benchmark to test the accuracy of ab initio calculations. The most recent and sophisticated studies by Sadlej et al.[18] and Lane et al.[20] calculated D_0 of 3.990 kcal/mol (1396 cm^{-1}) and 4.20 kcal/mol (1469 cm^{-1}), respectively. Both papers acknowledge that the calculations typically give binding energies for van der Waals complexes that are too low by 10−15%, mainly due to an underestimation of the dispersion component of the interaction energy. Sadlej tried to recover some of this by recomputing at the MP2 level in the larger aug-cc-pVQZ basis and correcting for higher order correlation effects, as well as deformation energies and zero-point corrections from aug-cc-pVTZ. This recomputation leads to their "best" value of 4.149 kcal/mol (1450 cm^{-1}). The calculated D_0 from these two studies are thus quite close and lie about 6% below our measured D_0. The proximity of the calculations to our measurement may indicate that dispersion is less important in the NH_3-H_2O bonding than in more weakly bound complexes.

4.3. Fragments' Rovibrational State Populations and Predissociation Mechanism. We turn now to a discussion of the VP mechanism of NH_3-H_2O, and in particular compare it to the linear NH_3−acetylene dimer.[34] Although the large number of states generated in the dissociation of NH_3-H_2O for both fragments precludes a state-to-state analysis, some information can be gleaned from general trends in our results. The large number of states is noteworthy in itself. The NH_3 REMPI spectra show considerable population in all energetically allowed rovibrational states of the ammonia umbrella mode (ν_2), with the population fairly evenly distributed between the vibrational levels. This is in contrast to what was previously observed for the NH_3−acetylene complex, for which ammonia fragments were predominantly formed in $\nu_2 = 1$ and no ground-state ammonia fragments were observed. In addition, our simulations of the transitions from $\nu_2 = 1^+$ and 2^+ matched our observed spectra quite well assuming a Boltzmann distribution of rotational states truncated at the maximum allowed rotational level. This is also in contrast to the NH_3−acetylene case, for which the colder rotational temperatures (<150 K) suggest a restricted range of impact parameters accessed by the linear dimer. Although we could not measure directly the population of $\nu_2 = 1^-$ and 2^-, in analogy with NH_3−acetylene we expect their rotational distributions to be similar to the (+) components.

The imaging data provide information on the rovibrational state distributions in the water cofragment pair-correlated with specific $NH_3(\nu, J)$ states. The distributions shown in Figures 7−9 have several noteworthy features. The first is again the large number of water states observed. Although the large density of water states prevents us from unambiguously assigning exact populations to individual J_{KaKc} states, we can conclude that the entire range of energetically allowed rotational water states is populated. Had some K_aK_c levels been excluded, much more structure would have been observed in the images.

In general, assuming a smooth variation of rotational populations, the distributions show a gradual increase in population with increasing internal energy of the water fragment. This is in accord with the momentum gap law that predicts a preference for rotational excitation over translational energy release, as long as the angular momentum "load" is not too large.[34,35,50−54] For example, the lowest translational energy region in Figure 9 is correlated with $J_{KaKc} = 9_{63}$ and the highest J level of H_2O possible for any K_aK_c combination is $J = 11$. The water J_{KaKc} states correlated with ammonia in excited umbrella levels are even lower. Previous results for the H(D)Cl−acetylene system showed that the angular momentum load did not restrict the rotational states of acetylene for $J < 20$.[35] We therefore expect no angular momentum restrictions on the rotational levels of water, particularly considering the large range of impact parameters that can be accessed by the zero-point motion of the floppy NH_3-H_2O dimer. We also note that, although the water state populations generally increase smoothly with water internal energy, at the highest allowed energies for each image we observe some significant state-to-state fluctuations. However, given the presence of background signal between peaks (see Figure 7), we cannot exclude the possibility that these fluctuations result from contributions of overlapping NH_3 transitions.

Referring to Ewing's propensity rules that favor excitation of vibrational levels to minimize translational energy release,[50,51] we find our results for NH_3 in $\nu_2 = 0^+$ quite surprising. For low rotational levels of ground-state ammonia ($J = 0-5$), population in the bending mode of the water cofragment is energetically allowed (Figure 3), resulting in translational energy release of <350 cm^{-1} for the rotationless state of ammonia. Studies on other hydrogen-bonded dimers have shown evidence of interaction between the bound OH stretch of water and the water bending modes, facilitated perhaps by the intermolecular modes.[55−57] We have therefore expected a strong preference for populating this mode. However, as shown in Figure 9, there is no clear evidence for water bend excitation. In fact, even if those levels marked in Figure 9 as possibly belonging to $H_2O(010)$ were all in this state, their fractional population would still be quite low in comparison with those levels that must belong to $H_2O(000)$. The same is true for the image we took by monitoring $NH_3(J = 3)$. This is all the more surprising given that product pairs in which both the ammonia and water are in their ground vibrational states can have translational energies as high as

$\sim$1800 cm^{-1}. In contrast, in the NH_3-acetylene case the maximum observed translational energy release was <150 cm^{-1}. Why the $H_2O(010)$ state is not populated significantly is not yet clear, especially since its energy is almost the same as two quanta in the ammonia umbrella mode (see Figure 3). We also see no evidence for population of the NH_3 asymmetric stretch (ν_4) in the REMPI spectra, which we would expect to be populated if the distribution of states was statistical.

While there has not been a previous study of the predissociation of NH_3-H_2O, the results of Fraser and Suenram[29] offer some insights into possible mechanisms. Their investigations of the ammonia symmetric bend absorption spectrum lead to two interesting observations: (1) there are many more observed sub-bands than can be explained just by tunneling motions in the dimer and (2) the ammonia bend in the dimer is blue-shifted by about 70 cm^{-1} from that in free ammonia. They have proposed that the extra sub-bands arise from coupling of the ammonia bend to the low-frequency intermolecular modes. Blue-shifts of the NH_3 bending mode in hydrogen-bonded complexes have previously been rationalized by a weakening of the hydrogen bond upon bending excitation.[58] Fraser and Suenram attribute this weakening to the observed decrease in the electric dipole moment of free NH_3 upon excitation to ν_2.[59] As discussed above, our data do not indicate a weakening; however, the extra sub-bands coupled with the blue-shift clearly suggest a significant coupling between the hydrogen bond and the ammonia symmetric bend.

On the basis of the available information, we can offer the following scenario for VP following excitation of the bound OH stretch in NH_3-H_2O. The floppy nature of the dimer and relatively strong hydrogen bond can facilitate more efficient energy flow and dissociation from a range of impact parameters.[34,35] This would explain the broad distribution of rotational levels in the products, which is restricted only by energy conservation, and the more democratic distribution among the ν_2 levels in ammonia. However, to achieve VP, efficient coupling to the intermolecular dissociation coordinate must take place, with the observed product states deriving predominantly from channels for which couplings to the hydrogen-bond dissociation coordinate are strongest. The spectroscopic studies show that the symmetric bend of ammonia is coupled to the intermolecular modes and the hydrogen bond. If this coupling is significantly stronger than for the water bend, the ammonia fragments would tend to be vibrationally excited, even though they are less favored by Ewing's propensity rules than the water bend. The way the system minimizes translational energy release in this case is by populating preferentially the higher rotational levels of water. Because the rotational constants of water are large, it takes only up to $J = 9$ to minimize the momentum gap, an angular momentum load that is quite reasonable. In the absence of a potential energy surface for the dimer, a more conclusive interpretation cannot be offered at present.

5. Summary

The state-to-state VP of the hydrogen-bonded NH_3-H_2O dimer was studied following excitation of the bound OH stretch. VMI and REMPI were used to determine product energy distributions. Following vibrational excitation of the bound OH stretch fundamental, ammonia fragments were detected by 2 + 1 REMPI via the $\tilde{B}^1E'' \leftarrow \tilde{X}^1A_1'$ transition. REMPI spectra show that NH_3 is produced with excitation of the symmetric bend (ν_2 umbrella mode), as well as in the ground vibrational state. Each band is quite congested, indicating population in a large number of rotational states. For NH_3 with ν_2 excitation the rotational energy extends to the highest allowed by conservation of energy and can be approximately described by a truncated Boltzmann-like distribution. The fragments' c.m. translational energy distributions were determined from images of selected rotational levels of ammonia with zero, one, or two quanta in ν_2 and were converted to rotational state distributions of the water cofragment. All the distributions could be fit well when using a dimer dissociation energy of $D_0 = 1538 \pm 10$ cm^{-1}. The rotational distributions in the water cofragment pair-correlated with specific rovibrational states of ammonia were broad and encompass all the J_{KaKc} states allowed by energy conservation. A detailed analysis of pair-correlated state distributions was complicated by the highly congested ammonia REMPI spectrum and the large number of water rotational states available, but the data suggest that the water rotational populations increase with decreasing translational energy. There is no evidence for ammonia products in the asymmetric bend (ν_4) or water products with excitation of the bend (ν_2). Apparently, the most efficient dissociation route involves coupling of states with ammonia symmetric bend excitation to the hydrogen-bond coordinate. The excitation of water bend is not a major channel even though population of the ground state of water leads to significant translational energy release. A more definitive mechanism must await dynamical calculations on the NH_3-H_2O potential energy surface.

We end by pointing out that the ammonia−water system has attracted much recent interest in the astrophysical and astrochemical communities because of its presence in icy bodies in the solar system.[7−11] Therefore, studies of energy flow and VP in mixed cyclic trimers as well as larger clusters would be enlightening.

Acknowledgment. This work is supported by the U.S. National Science Foundation. The authors thank Colin Western for his generous help in simulating the ammonia REMPI spectrum and Anthony J. McCaffery for stimulating discussions on the VP mechanism.

References and Notes

(1) Oudejans, L.; Miller, R. E. *Annu. Rev. Phys. Chem.* **2001**, *52*, 607.
(2) Reisler, H. *Annu. Rev. Phys. Chem.* **2009**, *60*, 39.
(3) Chan, J. P.; Giauque, W. F. *J. Phys. Chem.* **1964**, *68*, 3053.
(4) Lemmon, R. M. *Chem. Rev.* **1970**, *70*, 95.
(5) Cavazzoni, C.; Chiarotti, G. L.; Scandolo, S.; Tosatti, E.; Bernasconi, M.; Parrinello, M. *Science* **1999**, *283*, 44.
(6) Donaldson, D. J. *J. Phys. Chem. A* **1999**, *103*, 62.
(7) Brown, M. E.; Calvin, W. M. *Science* **2000**, *287*, 107.
(8) Cook, J. C.; Desch, S. J.; Roush, T. L.; Trujillo, C. A.; Geballe, T. R. *Astrophys. J.* **2007**, *663*, 1406.
(9) Moore, M. H.; Ferrante, R. F.; Hudson, R. L.; Stone, J. N. *Icarus* **2007**, *190*, 260.
(10) Verbiscer, A. J.; Peterson, D. E.; Skrutskie, M. F.; Cushing, M.; Helfenstein, P.; Nelson, M. J.; Smith, J. D.; Wilson, J. C. *Icarus* **2006**, *182*, 211.
(11) Zheng, W.; Jewitt, D.; Kaiser, R. I. *Astrophys. J. Suppl. Ser.* **2009**, *181*, 53.
(12) Moore, T. S.; Winmill, T. F. *J. Chem. Soc.* **1912**, *101*, 1635.
(13) Dykstra, C. E.; Andrews, L. *J. Chem. Phys.* **1990**, *92*, 6043.
(14) Janowski, T.; Jaszunski, M. *Int. J. Quantum Chem.* **2002**, *90*, 1083.
(15) Kohler, G.; Janoschek, R. *J. Phys. Chem.* **1987**, *91*, 2051.
(16) Langlet, J.; Caillet, J.; Berges, J.; Reinhardt, P. *J. Chem. Phys.* **2003**, *118*, 6157.
(17) Latajka, Z.; Scheiner, S. *J. Phys. Chem.* **1990**, *94*, 217.
(18) Sadlej, J.; Moszynski, R.; Dobrowolski, J. C.; Mazurek, A. P. *J. Phys. Chem. A* **1999**, *103*, 8528.
(19) Rzepkowska, J.; Uras, N.; Sadlej, J.; Buch, V. *J. Phys. Chem. A* **2002**, *106*, 1790.
(20) Lane, J. R.; Vaida, V.; Kjaergaard, H. G. *J. Chem. Phys.* **2008**, *128*, 034302.
(21) Yeo, G. A.; Ford, T. A. *Can. J. Chem.* **1991**, *69*, 632.
(22) Huang, N.; MacKerell, A. D. *J. Phys. Chem. A* **2002**, *106*, 7820.

(23) Rappe, A. K.; Bernstein, E. R. *J. Phys. Chem. A* **2000**, *104*, 6117.
(24) Tuma, C.; Boese, A. D.; Handy, N. C. *Phys. Chem. Chem. Phys.* **1999**, *1*, 3939.
(25) Engdahl, A.; Nelander, B. *J. Chem. Phys.* **1989**, *91*, 6604.
(26) Nelander, B.; Nord, L. *J. Phys. Chem.* **1982**, *86*, 4375.
(27) Yeo, G. A.; Ford, T. A. *Spectrochim. Acta, Part A* **1991**, *47*, 485.
(28) Kuma, S.; Slipchenko, M. N.; Momose, T.; Vilesov, A. F. *Chem. Phys. Lett.* **2007**, *439*, 265.
(29) Fraser, G. T.; Suenram, R. D. *J. Chem. Phys.* **1992**, *96*, 7287.
(30) Herbine, P.; Dyke, T. R. *J. Chem. Phys.* **1985**, *83*, 3768.
(31) Slipchenko, M. N.; Kuyanov, K. E.; Sartakov, B. G.; Vilesov, A. F. *J. Chem. Phys.* **2006**, *124*, 241101.
(32) Stockman, P. A.; Bumgarner, R. E.; Suzuki, S.; Blake, G. A. *J. Chem. Phys.* **1992**, *96*, 2496.
(33) Li, G.; Parr, J.; Fedorov, I.; Reisler, H. *Phys. Chem. Chem. Phys.* **2006**, *8*, 2915.
(34) Parr, J. A.; Li, G.; Fedorov, I.; McCaffery, A. J.; Reisler, H. *J. Phys. Chem. A* **2007**, *111*, 7589.
(35) Pritchard, M.; Parr, J.; Li, G.; Reisler, H.; McCaffery, A. J. *Phys. Chem. Chem. Phys.* **2007**, *9*, 6241.
(36) Ashfold, M. N. R.; Dixon, R. N.; Stickland, R. J.; Western, C. M. *Chem. Phys. Lett.* **1987**, *138*, 201.
(37) Western, C. M. PGOPHER, A Program for Simulating Rotational Structure; University of Bristol: Bristol, U.K., 2007. http://pgopher.chm-.bris.ac.uk.
(38) Cottaz, C.; Kleiner, I.; Tarrago, G.; Brown, L. R.; Margolis, J. S.; Poynter, R. L.; Pickett, H. M.; Fouchet, T.; Drossart, P.; Lellouch, E. *J. Mol. Spectrosc.* **2000**, *203*, 285.
(39) Eppink, A. T. J. B.; Parker, D. H. *Rev. Sci. Instrum.* **1997**, *68*, 3477.
(40) Dribinski, V.; Potter, A. B.; Fedorov, I.; Reisler, H. *J. Chem. Phys.* **2004**, *121*, 12353.
(41) Dribinski, V.; Ossadtchi, A.; Mandelshtam, V. A.; Reisler, H. *Rev. Sci. Instrum.* **2002**, *73*, 2634.
(42) Demyanenko, A. V.; Dribinski, V.; Reisler, H.; Meyer, H.; Qian, C. X. W. *J. Chem. Phys.* **1999**, *111*, 7383.
(43) Liu, C. L.; Hsu, H. C.; Ni, C. K. *Phys. Chem. Chem. Phys.* **2005**, *7*, 2151.
(44) Parker, D. H.; Eppink, A. T. J. B. *J. Chem. Phys.* **1997**, *107*, 2357.
(45) Lanquetin, R.; Coudert, L. H.; Camy-Peyret, C. *J. Mol. Spectrosc.* **1999**, *195*, 54.
(46) Judge, R. H.; Clouthier, D. J. *Comput. Phys. Commun.* **2001**, *135*, 293.
(47) McCoy, A. B.; Fry, J. L.; Francisco, J. S.; Mollner, A. K.; Okumura, M. *J. Chem. Phys.* **2005**, *122*, 104311.
(48) Hilpert, G.; Fraser, G. T.; Pine, A. S. *J. Chem. Phys.* **1996**, *105*, 6183.
(49) Paul, J. B.; Provencal, R. A.; Chapo, C.; Petterson, A.; Saykally, R. J. *J. Chem. Phys.* **1998**, *109*, 10201.
(50) Ewing, G. E. *J. Chem. Phys.* **1979**, *71*, 3143.
(51) Ewing, G. E. *J. Chem. Phys.* **1980**, *72*, 2096.
(52) Ewing, G. E. *J. Phys. Chem.* **1987**, *91*, 4662.
(53) Osborne, M. A.; McCaffery, A. J. *J. Chem. Phys.* **1994**, *101*, 5604.
(54) McCaffery, A. J. *Phys. Chem. Chem. Phys.* **2004**, *6*, 1637.
(55) Nizkorodov, S. A.; Ziemkiewicz, M.; Nesbitt, D. J.; Knight, A. E. *J. Chem. Phys.* **2005**, *122*, 194316.
(56) Robertson, W. H.; Weddle, G. H.; Kelley, J. A.; Johnson, M. A. *J. Phys. Chem. A* **2002**, *106*, 1205.
(57) Roscioli, J. R.; Diken, E. G.; Johnson, M. A.; Horvath, S.; McCoy, A. B. *J. Phys. Chem. A* **2006**, *110*, 4943.
(58) Fraser, G. T.; Nelson, D. D.; Charo, A.; Klemperer, W. *J. Chem. Phys.* **1985**, *82*, 2535.
(59) Ueda, Y.; Iwahori, J. *J. Mol. Spectrosc.* **1986**, *116*, 191.

JP904566W